IJCRT.ORG ISSN : 2320-2882

INTERNATIONAL JOURNAL OF CREATIVE RESEARCH THOUGHTS (IJCRT)

An International Open Access, Peer-reviewed, Refereed Journal

Synthesis Of Silicon Nitride And Used For Photocatalytic Degradation Of Methylene Blue

Dhanashree Hole[1], Manisha Sapkal[2] Jayshree Waghmode[1], Ramchandra Sapkal[1]*

[1]Department of Physics, Tuljaram Chaturchand College of Arts, Science and Commerce, Baramati, Affiliated to Savitribai Phule, Pune University Pune , 413102, (MH) India.

[2]Department of Microbiology, Balasaheb Desai College Patan , Dist Satara, 415206 , (MH) India

Abstract:

Silicon nitride (Si_3N_4) was synthesized from silicon metal powder in a nitrogen atmosphere at 1200ºC temperature by nitridation method. Synthesized material is characterized by X-ray diffraction (XRD) analysis and shows hexagonal structure. The XRD pattern matched with the standard JCPDS Card no. 01-082-0695. Theoretical investigation is carried out using Density functional theory (DFT) and revealed a bandgap of 3.33eV. The photocatalytic degradation efficiency 89.90% of Si_3N_4 was evaluated using methylene blue (MB), achieving a degradation rate constant $K=1.035\times10^{-4}sec^{-1}$. The synthesized Si_3N_4 exhibited excellent photocatalytic activity, making it a promising material for water purification application.

Keywords: Si_3N_4 Powder, Direct Nitridation, XRD, DFT.

1. Introduction

Silicon nitride ceramicarebeing used for systems parts subjected to high temperatures and high stresses [1]. It has applications as insulations, radiant burners, catalyst support, adsorption-seperation, solar cells, filters, sensing devices, wastewater treatment energy storage, pigments, coatings, thermostable materials and reinforcement for foams for the structural applications. In biomedical areas like hard tissue generation, cement, drug delivery, delivery of antibiotics, protein delivery, bioreactors, filler or packing materials the silicon nitride with porous nature is applicable. It has important application as a powerful killer of the SARS-Cov-2 virus[2-6].Today whole world is facing to a very big issue which is water pollution caused by release of uncontrolled dyes in river and it affect us by inducing Carcinogenic, teratogenic, Mutagenic effect[7]. By photocatalytic degradation, organic pollutant can be degradeat ambient temperature and gives byproduct water and CO_2. Photocatalytic process is induced by irradiation of semiconductor. Therefore there is excitation of free electron in the valance band, then these electron migrate to conduction band leaving holes in valence band[8] resulting in the production of electron-hole pair that move to the surface of the semiconductor. The induce hole and electron then induce the production of hydroxide radicals(OH) and superoxide radicals (O^{-2}) which are very reactive and promote the oxidation of organic pollutant into H_2O and CO_2[9-11]. Beside metal oxide and carbon nitrides have shown attractive photocatalytic acivity in the visible light region [12]. Function properties of the material were evaluated in terms of its photocatalytic efficiency for removal of Methylene Blue under visible light irradiation[13]. Silicon nitride due to its excellent high temperature property it is known as the ‘all round champion’ of ceramic material and therefore its applications include ball bearing for machine tools, cutting tool for metal manufacturing, forming, machining [14-16]. For production of silicon nitride at commercial level direct nitridation of silicon method is used. Its ability to withstand extreme

environments and maintain performance under high stress conditions has established. It is a material of significant interest of both academic and industrial research. The specific properties of silicon metal powder such as a particle size distribution, purity, surface area can be tailored to meet the requirements of different application. Additionly different grade of silicon metal powder may have varying characteristic to suit specific industrial processes. Silicon nitride with porous nature have unique characteristic properties such as low density, high porosity, ample interior space, high surface area, high and reproducible performance [17-19]. Silicon nitride can be synthesis via different method such as self propagating high temperatures synthesis[20], carbothermal nitriding of silicon dioxide[21], diimide synthesis by reacting silicon tetrachloride or monosilane [22], plasma chemical synthesis such as plasma enhanced chemical vapour deposition[23], excimer laser induced reactions of silane-ammonia mixture[24], pyrolysis of organo-silicon compounds[25], Sol-gel processing of polymreric precursors[26] anddirect nitriding of silicon powder[27]. In this work, we present the synthesis and photocatalytic performance of silicon nitride material prepared by using silicon metal powder and nitrogen gas. The microstructure and crystalline structure of the resulting material were determined by FESEM coupled with energy dispersive X-Ray spectroscopy(EDAX), X-Ray diffraction.

2. Materials and Methods

Synthesis of Si_3N_4

The Si_3N_4 is prepared by heating powdered silicon with purity 98.50% and molecular weight 28.09 gm/mol at 1200^0C in a nitrogen environment.

$$3Si + 2N_2 \rightarrow Si_3N_4 \quad \text{- - - - - -} \quad (1)$$

Without an catalyst the reaction is complete after seven hours. Silicon nitride is synthesized by direct nitridation method. The direct nitridation method carried out in muffle furnace.

3. Results and discussions

I. X-Ray Diffraction:

The crystalline structure of silicon nitride was characterized by the X-ray diffraction using CuKα radiation as the X-ray monochromatic source. The XRD patterns of a silicon nitride synthesized samples are shown in Fig. 1. And the detailed diagram shows that the peak positions of Si_3N_4 are at 13.44°, 23.41°, 27.10°, 33.70°, 36.10^0, 41.43^0, 47.93^0, 49.93^0, 52.21^0, 57.94^0, 61.36^0, 64.02^0, 64.89^0, 70.18^0, 73.49^0, 74.91^0, and 75.73^0 corresponding to the (100), (110), (200), (101), (120), (201), (220), (310), (301), (221), (320), (002), (410), (321), (141), (330) and (122) crystal planes respectively. While prominent peak are present at 13.44^0 (100), 23.41°(110), 27.10°(200), 33.70°(101), 36.10^0(120), 52.21^0(301), 70.18^0(321).

The lattice parameters and for hexagonal phase it was determined by using the equation given as follow

$$\frac{1}{d^2} \equiv \frac{4}{3}\left(\frac{h^2+hk+k^2}{a^2}\right) + \frac{l^2}{c^2} \quad \text{- - -- - - -} \quad (2)$$

For hexagonal lattice, $a = b \neq c$. In the above relation, d is their interplanar distance and h, k, l are miller indices of reflector planes appearing on the diffraction spectrum.

The obtained average lattice constants were found to be a =7.6018Å, b=7.6018Å, and c= 2.9071Å. These values are consistent with standard JCPDS reference data. The average crystallite size (D) of the prepared films was calculated by the Scherrer formulation,

$$D = \frac{k\lambda}{\beta cos\theta} \quad \text{- - - -- - - - - -} \quad (3)$$

Where k is the constant term with value k= 0.94,λ is wavelength of x-ray (= 1.5406 Å), β is the full width at half maxima of diffraction peak, and θ is the Bragg's angle. The average crystallite size of the Si_3N_4 sample was 27 nm. The interplanar d-spacing were calculated by the following formulation [28],

$$n\lambda = 2dsin\theta \quad \text{- - - - - - - - -} \quad (4)$$

Where,d is the interplanar spacing, $\theta$is the Bragg's angle,$n$is the order of diffraction (usually n = 1), $\lambda$and is the wavelength of the x-ray used (here, λ = 1.5406 Å). All the values of d-spacing corresponding to diffraction peaks are tabulated in table 1.

$$\text{Texture coefficient } (TC_{hkl}) = \frac{\frac{I(hkl)}{I_o(hkl)}}{\frac{1}{N}\sum\frac{I(hkl)}{I_o(hkl)}} \quad \text{- - - - - - -} \quad (5)$$

Where, I is the measured intensity, I_0 the standard intensity of the Si_3N_4 and N the number of (hkl) diffraction peaks. Sample with a randomly oriented crystallite reveals TC_{hkl} = 1, and if TC_{hkl}>1, then there is bigger abundance of crystallite orientation. From the definition, however, it is obvious that the deviation of TC from implying an enlargement in the number of grains along the plane [29]. The TC values for the eight major diffraction planes of (100), (110), (200), (101), (120), (201), (301), (321)are listed in Table 1.and depicted in Fig.1. The dislocation density (d) which signifies the amount of defects in the Si_3N_4 is calculated using the formula [30]:

$$\text{Dislocation density } \boldsymbol{(\delta)} = \frac{1}{D_{DS}^2} = \frac{1}{D_{W-H}^2} \quad \text{- - - - - - - - -} \quad (6)$$

Where, D_{DS} and D_{W-H} are the particle sizes calculated by DS and W–H formula. To estimate the micro-strain effect, the Williamson–Hall (W–H) method was chosen; thus, the Debye–Scherrer (DS) equation does not include the strain effect and the instrumental effect [31, 32]. This micro-strain effect is illustrated with the help of W–H plot, as shown in Fig. 2. The peak broadening of the XRD patterns is a result of the particle size and micro-strain (ϵ). Lorentzian profile of the peaks splits the two contributions given by $\beta = \beta_D + \beta_S$, where β_D and β_S are the full width at half maxima of the particle size and standard profiles, respectively. The W–H equation may be inscribed in equation (7) [33],

$$\beta Cos\theta = \frac{K\lambda}{D} + 4\epsilon Sin\theta \quad \text{- - - - - - - - -} \quad (7)$$

where θ is the Bragg diffraction angle, K is the shape factor,λ is the wavelength of X-ray and D is the crystallite size. The W–H plot is illustrated with Sinθ versus βCosθ for Si_3N_4, and the plot lies along a straight line. The micro-strain (ϵ) is determined from the slope of the illustrated graph (Fig.2). The reciprocal of the intercept of the fitted straight line indicates the D_{DS} including the strain effect. The details of the estimation of the parameters from the W–H plot are shown in Table 2. The micro strains (ϵ)of the Si_3N_4 was 0.064574. The internal micro strain can readily lead to the creation of defect.The stress (σ) of the Si_3N_4can be calculated using the relation: σ = ϵE, where E is the Young's modulus for $Si_3N_4$with value being 260 GPa.The stress (σ) of the Si_3N_4 was 16.7892 GPa. C by a ratio for hexagonal crystal structure of the Si_3N_4found 0.3824.

II. Field Emission Scanning Electron Microscopy:

The Surface morphology of the silicon nitride was analyzed using field emission scanning electron microscopy (FESEM) Figure 3. FESEM analysis of silicon nitride (Si_3N_4) reveals its microstructure, showing cubical rod like structures for Si_3N_4.

III. Energy-dispersive X-ray spectroscopy:

Energy-dispersive X-ray spectroscopy (EDX): Si_3N_4shown hexagonal rods formed. Besides, the EDS mapping spectrum shows that there are related C, N, Si and O elements. But in the Si_3N_4, it contain Si and N as major elements as given in Figure 4.

IV. Fourier Transform Infrared Spectroscopy:

FTIR spectra were obtained with a spectrometer in the range of 500–2000 cm^{-1}.

FTIR spectrum of the Si_3N_4, as shown in Figure 5, features a band at approximately 560 cm^{-1}, which corresponds to the Si-N group. Additionally, the band at 1010 cm^{-1} is attributed to the Si-O-Si bond and at 1250 cm^{-1} which correspond to C-N bond.

Ⅴ. Density Functional Theory:

The band structure of Si_3N_4 was determined using Density Functional Theory.

The electrical structure and optical properties of the Si_3N_4 were calculated via DFT calculations.

From calculated band structure the top of valence band and the bottom of conduction band were shown to be localized at different points on the surface of the brillouin zone of the hexagonal lattice, namely along symmetry line Γ located top of valence band and at the symmetry point Γ located bottom of conduction band (Fig.6). As shown in figure 12.54 eV of the energy scale shows the position of the Fermi level. This in their turn indicates that Si_3N_4 is an direct gap semiconductor with the 3.33 eV. The calculated valence bands below the Fermi energy agree well with other first principle studies. The band gap of Si_3N_4 was found to be close to 3.33 eV through first-principles calculations using the local density approximation (LDA) (Lu, *et* al., 2013). From the Γ-point, one can see that only the γ-phase is a direct band-gap material, however, other phases show indirect band-gap (in agreement with observations) [36]. The energies are measured from the top of the valence band.

4. Degradation of Methylene Blue

Absorbance spectra were obtained with a UV-Vis spectrophotometer in the wavelength range of 200–800 nm. The optical properties of the samples were studied by UV visible spectroscopy. All samples showed a visible light response (Fig.7). However, the absorption wavelength of sample Si_3N_4in visible light is about 400 nm (the corresponding band gap is 3.33 eV).

Generally speaking, enhancing the absorption intensity of visible light can improve the utilization rate of light and may improve the photocatalytic performance of materials.

The photocatalytic degradation was carried out under visible light using UV lamp as an irradiation source. The concentration of methylene blue (MB) in the aqueous solution was set to 1 ppm a value that is commonly used in relevant literature. For each photocatalytic experiment, 100 mL of this solution was used. The irradiation lamp was positioned directly above the solution and the walls of the beaker, which were obscured to prevent any potential contribution from natural light. The experimental setup is depicted in Figure 1. After this period, the light was turned on and the solution was continuously irradiated for 4h. And after each 30 min. 5 ml solution was taken out to determine degradation.

The degradation efficiency η of the Si_3N_4 was calculated by applying the Beer–Lambert law, which states that the absorbance of MB is proportional to the concentration, as described in Equation (8) [34,35]:

$$\eta\% = \left[\frac{(C_\circ - C)}{C_\circ}\right] \times 100\% = \left[\frac{(A_\circ - A)}{A_\circ}\right] \times 100\% \text{ - - - -- -- - - - - -} \qquad (8)$$

where, C_0 and A_0 are the MB initial concentration (mg/L) and absorbance, and C and A are the concentration and absorbance at time t, respectively (Fig 8) . The photocatalytic degradation efficiency 89.90% of Si_3N_4 was evaluated using methylene blue (MB), achieving a degradation rate constant $K=1.035\times10^{-4}sec^{-1}$.

5. Conclusion:

In conclusion, hexagonal Silicon nitride was successfully synthesized by simple and low-cost Direct Nitridation approach. Si_3N_4 shows the cubical rod like morphology. Carried out first principle calculation for investigation electronic band structure and optical properties of Si_3N_4 indicate that this compound is direct band gap compound. The direct gap at the Γ-point is 3.33 eV. The synthesized Si_3N_4 exhibited excellent photocatalytic activity, making it a promising material for water purification application.

References

1. Klemm, H. Silicon nitride for high temperature applications. *J. Am. Ceram. Soc.* **2010**, *93*, 1501–1522.
2. Cochran JK. Ceramic hollow spheres and theirapplications. Curr Opin Solid State Mater Sci. 1998;3(5):474–479.
3. Bae E, Chah S, Yi J. Preparation and characterization ofceramic hollow microspheres for heavy metal ionremoval in wastewater. J Colloid Interface Sci.2000;230(2):367–376.
4. Klein TY, Treccani L, Rezwan K. Ceramic microbeads asadsorbents for purification technologies with highspecific surface area, adjustable pore size, and morphology obtained by ionotropic gelation. J Am CeramSoc. 2012;95(3):907–914.
5. Li Y, Wang S, Hao P, et al. Soft-templated formation ofdouble-shelled ZnO hollow microspheres for acetonegas sensing at low concentration/near roomtemperature. Sens Actuators B Chem. 2018;273:751–759.
6. Cao J, Wang S, Zhang H, et al. Facile construction ofCo3O4 porous microspheres with enhanced acetonegas sensing performances. Materials Science inSemiconductor Processing. 2019;101:10–15
7. Liu, Q. Pollution and Treatment of Dye Waste-Water. *IOP Conf. Ser. Earth Environ. Sci.* **2020**, *514*, 052001.
8. Kouamé, N.A.; Robert, D.; Keller, V.; Keller, N.; Pham, C.; Nguyen, P. Preliminary Study of the Use of β-SiC Foam as a Photocatalytic Support for Water Treatment. *Catal. Today* **2011**, *161*, 3–7.
9. Hariganesh, S.; Vadivel, S.; Maruthamani, D.; Rangabhashiyam, S. Disinfection By-Products in Drinking Water: Detection and Treatment Methods. In *Disinfection By-products in Drinking Water*; Elsevier: Amsterdam, The Netherlands, 2020; pp. 279–304. ISBN 9780081029770.
10. Abebe, B.; Murthy, H.C.A.; Amare, E. Summary on Adsorption and Photocatalysis for Pollutant Remediation: Mini Review. *J. Encapsulation Adsorpt. Sci.* **2018**, *08*, 225–255.
11. Aziz, N.A.A.; Palaniandy, P.; Aziz, H.A.; Dahlan, I. Review of the Mechanism and Operational Factors Influencing the Degradation Process of Contaminants in Heterogenous Photocatalysis. *J. Chem. Res.* **2016**, *40*, 704–712.
12. Hao, Q.; Niu, X.; Nie, C.; Hao, S.; Zou, W.; Ge, J.; Chen, D.; Yao, W. A Highly Efficient G-C_3N_4/SiO_2 Heterojunction: The Role of SiO_2 in the Enhancement of Visible Light Photocatalytic Activity. Phys. Chem. Chem. Phys. **2016**, 18, 31410–31418.
13. Robert B. Heimann. Am Stadtpark 2A, D-02826 Görlitz, Germany.Silicon Nitride Ceramics: Structure, Synthesis, Properties, and Biomedical Applications.*Materials* **2023**,*16*(14),5142;https://doi.org/10.3390/ma16145142.
14. Riley, F.L. Applications of silicon nitride ceramics. Key Eng. Mater. **1996**, 122–124, 479–488. Riley, F.L. Silicon nitride and related materials. J. Am. Ceram. Soc. **2000**, 83, 145–265.
15. Petzow, G.; Herrmann, M. Silicon nitride ceramics. In High Performance Non-Oxide Ceramics II. Structure and Bonding; Jansen, M., Mingos, D.M.P., Haubner, R., Eds.; Springer: Berlin/Heidelberg, Germany, 2002; Volume 102, pp. 47–168.
16. Caruso F, Caruso RA, Möhwald H. Nanoengineering of inorganic and hybrid hollow spheres by colloidal templating. Science. 1998;282(5391):1111–1114.
17. Göltner CG. Porous solids from rigid colloidal templates: morphogenesis. Angew Chem. 1999;38(21):3155–3156.
18. Sun Y, Xia Y. Shape-controlled synthesis of gold and silver nanoparticles. Science. 2002;298(5601):2176–2179

19. Chukhlomina, L.N., Vitushkina, O.G. & Vereshchagin, V.I. Self-propagating high-temperature synthesis of silicon-nitride ceramic mix using ferro-silicon and ilmenite. *Glass Ceram* **67**, 277–280 (2011). https://doi.org/10.1007/s10717-011-9279-y
20. Alcalá M.D, C. Real & José M. Criado,Preparation of Si3N4 from carbothermal reduction of SiO employing the CRTA method https://doi.org/10.4028/www.scientific.net/MSF.383.25
21. Robert B. HeimannSilicon Nitride Ceramics: Structure, Synthesis, Properties, and Biomedical Applications https://doi.org/10.3390/ma16145142
22. M. Belyansky, M. ChaceOlegGluschenkov, J. Kempisty. Methods of producing plasma enhanced chemical vapor deposition silicon nitride thin films with high compressive and tensile stress. DOI:10.1116/1.2906259.
23. D. B. Beach,J. M. Jasinski. Excimer laser photochemistry of silane-ammonia mixtures at 193 nm. https://pubs.acs.org/doi/abs/10.1021/j100370a053.
24. Jiliang He, Mihai Scarlete, John F. HarrodSilicon Nitride and Silicon Carbonitride by the Pyrolysis of Poly(methylsiladiazane).https://doi.org/10.1111/j.1151-2916.1995.tb09076.x
25. Andrew L. Hector.Synthesis and processing of silicon nitride and related materials using preceramic polymer and non-oxide sol-gel approaches.https://doi.org/10.1016/j.ccr.2016.05.009
26. Cost-effective preparation of high-quality silicon nitride powders from silicon scrap through direct nitridation. Kati Raju, Seunghwan Moon, Minwook Kim ,Ha-Neul Kim, Hyun-Kwuon Lee, Jaehun Cho.https://doi.org/10.1016/j.ceramint.2023.08.161.
27. Modified Structural, Optical and Electrochemical Properties of Nickel Sulphide for Superior Supercapacitor Electrodehttps://doi.org/10.5281/zenodo.7763091.
28. Turgut G, Erdal S, Mehmet Y, Selim MC, Yılmaz MC, TurgutU, Refik D. The variation of the features of SnO2 and SnO2: F thin films as a function of V dopant. J Mater Sci Mater Electron.2014;25(6):2808
29. Tripathi A, Shukla RK. Blue shift in optical band gap of sol–gel derived Sn1-xZnxO2 polycrystalline thin film. J Mater Sci Mater Electron. 2013;24(10):4014.
30. Weibel A, Bouchet R, Boulc F, Knauth P. The problem of small particles: a comparison of methods for determination of particle size in nanocrystalline anatase powders. Chem Mater. 2005; 17(9):2378.
31. Markmann J, Yamakov V, Weissmu¨ller J. Validating grain size analysis from X-ray line broadening: a virtual experiment. Scripta Mater. 2008;59(1):15.
32. Williamson G, Hall W. X-ray line broadening from filed aluminium and wolfram. Acta Metall. 1953;1(1):22.
33. Soltani, N.; Saion, E.; Mahmood Mat Yunus, W.; Navasery, M.; Bahmanrokh, G.; Erfani, M.; Zare, M.R.; Gharibshahi, E. Photocatalytic Degradation of Methylene Blue under Visible Light Using PVP-Capped ZnS and CdS Nanoparticles. Sol. Energy **2013**, 97, 147–154.
34. Iram, M.; Guo, C.; Guan, Y.; Ishfaq, A.; Liu, H. Adsorption and Magnetic Removal of Neutral Red Dye from Aqueous Solution Using Fe3O4 Hollow Nanospheres. J. Hazard. Mater. **2010**, 181, 1039–1050.
35. E. Kasumova, A. Aslanova A: First Principle Calculation Electronic And Optical Properties Of Si_3N_4. Advanced Physical Research Vol.3, No.2, 2021, pp.104-107.

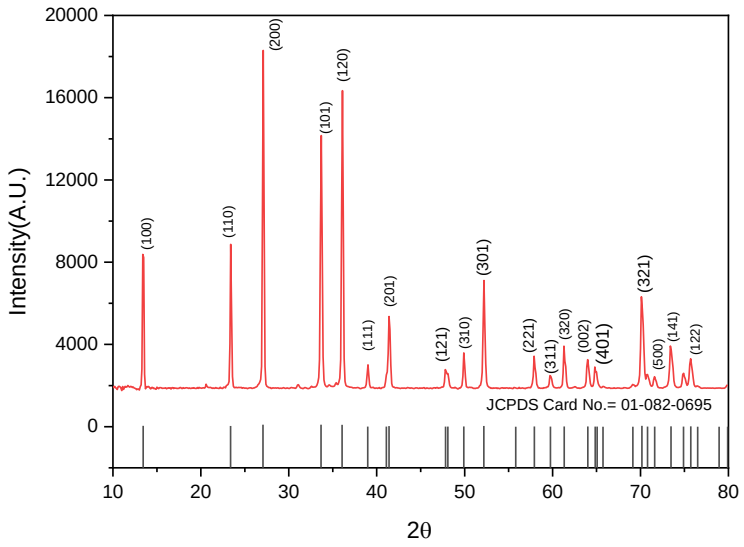

Fig.1. The XRD patterns of as synthesized Si_3N_4

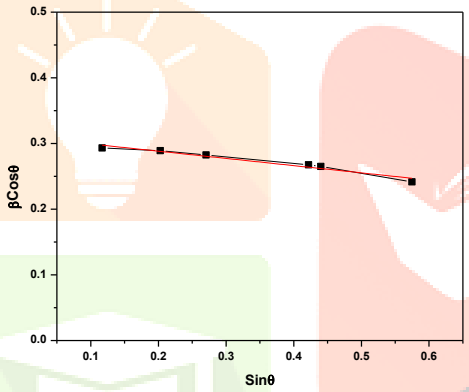

Fig. 2 Micro-strain effect curves of Si_3N_4

Table1. X-ray diffraction data for Crystalline Size, Dislocation Density, Texture Coefficient of the Si_3N_4

Sr No.	2θ	(hkl)	d-spacing[A^0]	Crystalline Size(D) nm	Dislocation Density(δ)(Lines.m-2)	Texture Coefficient(TC)
1	13.44	100	6.2833	27	0.0013	1.1449
2	23.41	110	3.800			1.3149
3	27.10	200	3.2916			1.1423
4	33.70	101	2.6593			0.8929
5	36.10	120	2.4882			1.1121
6	41.43	201	2.1789			0.7812
7	52.21	301	1.7514			0.9548
8	70.18	321	1.3402			0.6563

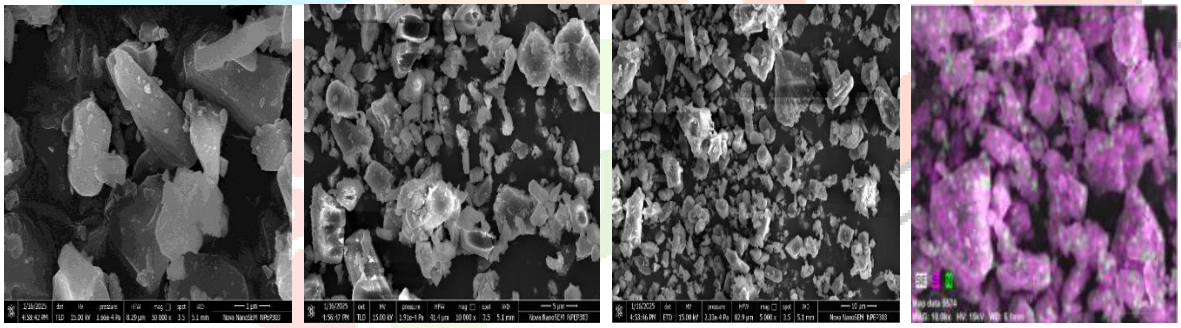

Fig.3. FE-SEM of Si_3N_4

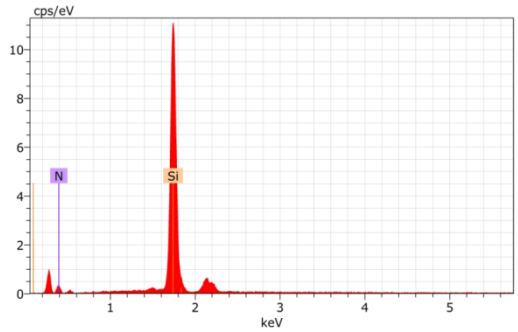

Fig.4. EDX of Si_3N_4

Sr.No	element	Atomic Percentage	Weight %
1	Si	65.92	79.50
2	N	34.08	20.50
Total		100	100

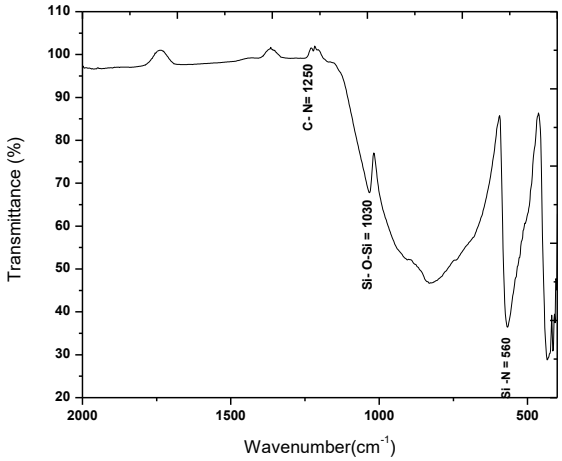

Fig.5. FTIR of Si_3N_4

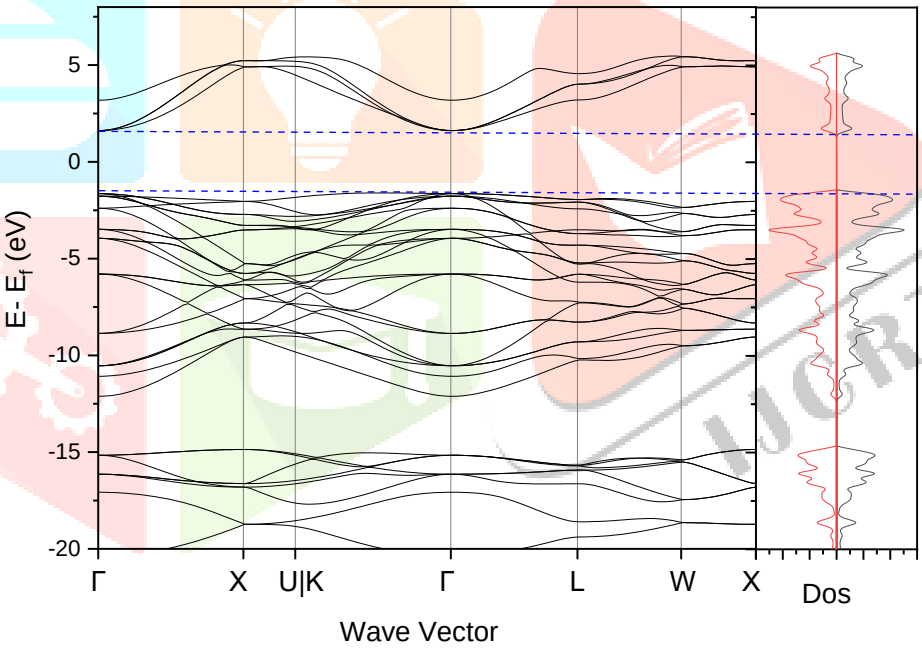

Fig.6. Band structure and Density of States of Si_3N_4

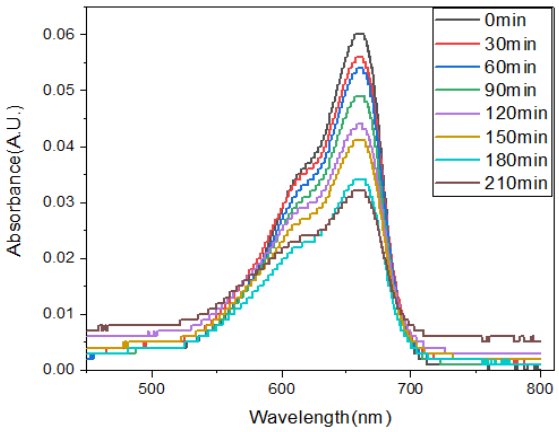

Fig.7. Photocatalytic degradation of Methylene Blue under UV irradiation.

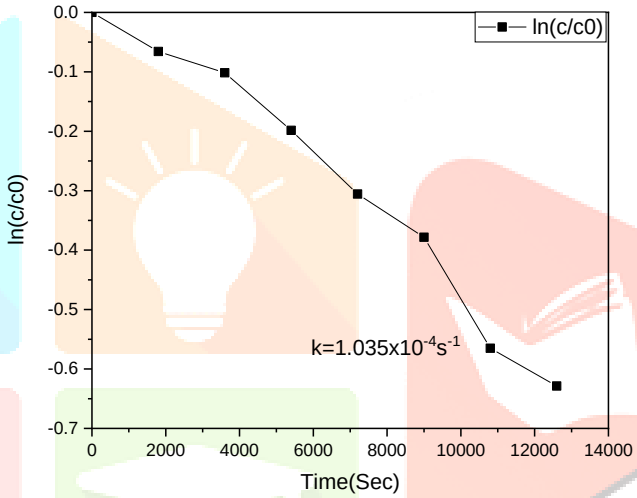

Fig.8. Rate constant of photo catalytic degradation of methylene blue